DOI: 10.1002/chem.200700568

Revealing Shape Selectivity and Catalytic Activity Trends Within the Pores of H-ZSM-5 Crystals by Time- and Space-Resolved Optical and Fluorescence Microspectroscopy

Eli Stavitski, Marianne H. F. Kox, and Bert M. Weckhuysen*[a]

Abstract: A combination of in-situ optical and fluorescence microspectroscopy has been employed to investigate the oligomerization of styrene derivatives occurring in the micropores of coffin-shaped H-ZSM-5 zeolite crystals in a space- and time-resolved manner. The carbocationic intermediates in this reaction act as reporter molecules for catalytic activity, since they exhibit strong optical absorption and fluorescence. In this way, reactant selectivity and restricted transition-state selectivity for 14 substituted styrene molecules can be visualized and quantified. Based on a thorough analysis of the time- and space-resolved UV/Vis spectra, it has been revealed that two main parameters affect the reaction rates, namely, the carbocation stabilization effect and the diffusion hindrance. The stabilization effect was tested by comparison of the reaction rates for 4-methoxystyrene versus 4-methylstyrene and in the series 4-bromo-, 4-chloro and 4-fluorostyrene; in both cases less electronegative substituents were found to accelerate the reaction. As to the steric effect, bulkier chemical groups bring down the reaction rate, as evident from the observation that 4-methoxystyrene is more reactive than 4-ethoxystyrene due to differences in their diffusivity, while heavily substituted styrenes, such as 3,4-dichlorostyrene and 2,3,4,5,6-pentafluorostyrene, cannot enter the zeolite pore system and therefore do not display any reactivity. Furthermore, β-methoxystyrene and *trans*-β-methylstyrene show limited reactivity as well as restricted reaction-product formation due to steric constraints imposed by the H-ZSM-5 channel system. Finally, polarized-light optical microspectroscopy and fluorescence microscopy demonstrate that dimeric styrene compounds are predominantly formed and aligned within the straight channels at the edges of the crystals, whereas a large fraction of trimeric carbocations along with dimeric compounds are present in the straight channels of the main body of the H-ZSM-5 crystals. Our results reinforce the observation of a non-uniform catalytic behavior within zeolite crystals, with specific parts of the zeolite grains being less accessible and reactive towards reactant molecules. The prospects and potential of this combined in-situ approach for studying large zeolite crystals in the act will be discussed.

Keywords: fluorescence · microspectroscopy · oligomerization · styrene · zeolites

Introduction

Zeolites represent a group of catalytic solids that are heavily used in petrochemical and refining industries. Since their discovery in the 1970s, zeolites with MFI topology, such as H-ZSM-5, have been utilized in different large-scale applications due to unique combination of the acidic properties and the pore architecture.[1] Examples include the alkylation of benzene or toluene with ethylene[2] and the oligomerization of light olefins.[3] Although the zeolite chemistry has been thoroughly studied, most characterization methods have focused on bulk chemical properties of H-ZSM-5 crystals and their relation with catalyst activity and selectivity. More specifically, IR spectroscopy of probe molecules adsorbed on powdered H-ZSM-5 samples has been used to relate Brønsted acid–base properties with activity in hydrocarbon cracking.[4] Taking the channel accessibility into consideration, the tapered element oscillating microbalance (TEOM) technique has been utilized to determine the uptake of different hydrocarbons into the pore system of H-ZSM-5, revealing fundamental insight into their diffusion properties.[5,6] However, as those methods are bulk techniques, they provide averaged information over the entire catalyst sample. To

[a] Dr. E. Stavitski, M. H. F. Kox, Prof. Dr. ir. B. M. Weckhuysen
Inorganic Chemistry and Catalysis group
Department of Chemistry, Utrecht University, Sorbonnelaan 16
3584 CA Utrecht (The Netherlands)
Fax: (+31) 30-251-1027
E-mail: b.m.weckhuysen@uu.nl

obtain more information from particles or grains on how the catalytic processes take place in distinct places of a catalyst, microspectroscopic techniques should be employed. To-date, a number of microscopic methods, such as IR, UV/Vis, Raman, and interference microscopy have been applied to study various steps in catalyst preparation and diffusion of organic compounds in the microporous materials.[7–11] Recently, two in-situ microspectroscopic techniques have been developed independently; these techniques allow us to study electrophilic substitution reactions in H-ZSM-5 crystals of micrometer dimensions in a space- and time-resolved manner. The first approach involves the use of an inverted confocal fluorescence microscope, as pioneered by Roeffaers et al.,[12,13] to investigate the alkylation of anisole and the self-condensation of furfuryl alcohol at room temperature.[14] In this manner, it was possible to visualize the reactivity dynamics of coffin-shaped H-ZSM-5 crystals as well as differences in reactivity patterns between different zeolite subunits. Furthermore, confocal microscopic imaging elegantly demonstrated that more conjugated oligomeric products are accumulated at the crystal edges. By this methodology detailed fundamental insights into the internal diffusion barriers for reagent adsorption within H-ZSM-5 crystals could be revealed. The second promising approach, developed by our group, involves the use of in-situ polarized-light optical microspectroscopy in combination with an in-situ cell, allowing a wide range of catalytic reactions under diverse experimental conditions, that is, both in the gas and liquid phase, with temperatures up to 1273 K. Making use of this experimental setup, it was possible to reveal the non-uniform catalytic behavior within H-ZSM-5 crystals.[15] More specifically, we have demonstrated for the oligomerization of different styrene molecules[16] at elevated temperatures that distinct pore geometries lead to different reaction products aligned within the straight pores of the zeolite material. Moreover, dimeric carbocation products are preferentially formed at the edges of the H-ZSM-5 crystals, whereas the main body of the zeolite crystal favors trimeric carbocation products.

In this work, we present a full account on the investigation of the oligomerization of 14 different styrene derivatives catalyzed by individual H-ZSM-5 crystals, revealing shape selectivity and activity trends within these zeolite materials. Together with the newly developed UV/Vis microspectroscopy setup, identical sets of experiments were performed with a confocal fluorescence microscope, which is, in contrast to the work of Roeffaers et al., in an upright configuration. This important modification allows extending the application window of the in-situ fluorescence technique to a wider range of experimental conditions. The use of the same in-situ reaction cell for both optical and fluorescence measurements ensures that the results obtained with the two spectroscopic techniques are fully comparable, illustrating the complementarity and power of both in-situ approaches for studying catalytic solids at work.

Results and Discussion

Figure 1 illustrates the combined approach developed in our laboratory based on polarized-light optical microspectroscopy and confocal fluorescence microscopy employed in an upright configuration, to study the reactivity of individual zeolite crystals making use of the same in-situ cell. In the case of the optical microspectroscopic setup, the light is focused onto the zeolite material through a high numerical aperture microscope objective lens and the reflected light is collected back by the objective lens and directed to the CCD-camera and/or to the optical fiber connected to a CCD UV/Vis spectrometer. Snapshots of zeolite crystals of micrometer dimensions along with time- and space-resolved optical absorption spectra can be measured. While this technique probes the optical absorption of the reagents and reaction products, the light emission can be monitored by means of confocal fluorescence microscopy. This method allows controllable depth of field or, in other words, the resolution along the vertical axis, which is achieved by using pinholes in the optical pathway to eliminate out-of-focus light. In this way, the thick specimen can be sectioned and

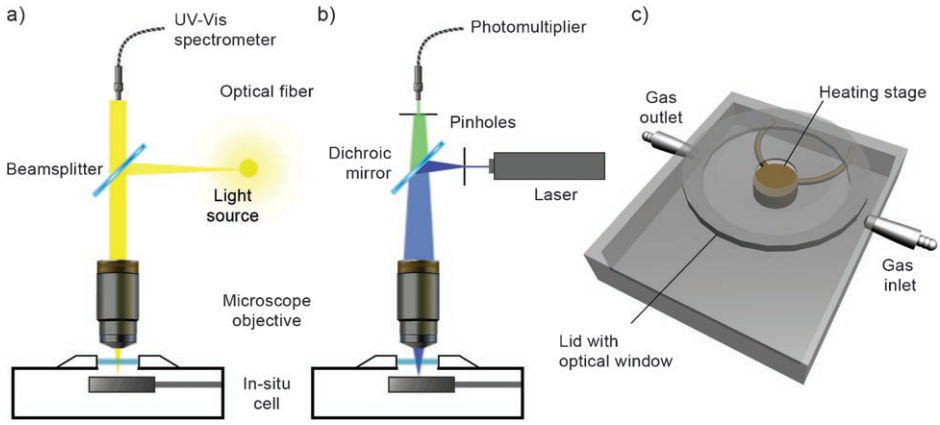

Figure 1. a) Schematic representation of the UV/Vis microspectroscopic setup. Light is focused onto the sample in the in-situ cell with a microscope objective. The optical fiber which is placed in the image plane, directs the reflected light from the ∅ 2 μm spot to a CCD UV/Vis spectrometer. Scanning over the sample is achieved by the motion of the microscope table. b) Confocal fluorescence microscopy setup, with the same reaction cell. Laser light is focused onto the sample and the fluorescence is collected by the microscope objective. Scattered light is cut off by a dichroic mirror. Pinholes in the optical path ensure that the out-of-focus light is eliminated. c) The in-situ spectroscopic cell used for the microscopic measurements, allowing to create controlled conditions for the catalytic reaction.

the three-dimensional spatial distribution of the fluorescence species can be reconstructed.

To investigate the influence of different substituent groups on the reactivity of the styrene oligomerization reaction within the channel system of acid-type zeolite materials, H-ZSM-5 crystals with typical dimensions of 100 μm × 20 μm × 20 μm, have been loaded with 14 different styrene derivatives (**1**–**14**; Table 1) from the liquid phase in the in-situ spectroscopic reaction cell. Optical absorption and fluorescence patterns have been evaluated as a function of reaction time as well as position within the zeolite crystal. In what follows, we will first discuss the characterization results obtained with optical microspectroscopy, illustrating the differences in reactivity between the different styrene molecules under study as well as the alignment of the formed carbocationic intermediates within the straight channels of the zeolite crystals. In a second part, we will illustrate that the same overall reactivity trend can also be deduced from the fluorescence microscopy results. Furthermore, we will show that, depending on the type of styrene molecule under study, different parts of the H-ZSM-5 crystal show different reactivity and reactant accessibility.

Table 1. Styrene derivatives under study, absorption band positions at the edge and the main body of H-ZSM-5 zeolite crystals exposed to the reagents at 373 K (**1**–**6**) and 473 K (**7**–**14**) and the reaction rate constants of the dimeric product formation (**D** in Scheme 1). Reaction rate constants correspond to the time evolution profiles presented in Figure 7.[a]

Compound	Band position [nm]		k
	edge	center	[$mol^{-1}s^{-1}$]
4-methoxystyrene (**1**)	585, 635	585, 630	0.05
4-ethoxystyrene (**2**)	585	585, 635	0.004
4-methylstyrene (**3**)	520, 570	520, 570, 625	0.005
4-bromostyrene (**4**)	560	520, 560, 620	0.05
4-chlorostyrene (**5**)	540, 580	540, 580, 630	0.009
4-fluorostyrene (**6**)	510, 550	510, 535, 570	0.0075
β-methoxystyrene (**7**)[b]	545	545	(0.02)
trans-β-methylstyrene (**8**)[b]	545	545	(0.02)
3-chlorostyrene (**9**)	N/A	N/A	N/A
2,3,4,5,6-penta-fluoro styrene (**10**)	N/A	N/A	N/A
α-methylstyrene (**11**)	N/A	N/A	N/A
3-trifluoromethylstyrene (**12**)	N/A	N/A	N/A
3,4-dichlorostyrene (**13**)	N/A	N/A	N/A
2,6-dichlorostyrene (**14**)	N/A	N/A	N/A

[a] The notation N/A (not applicable) applies to the styrene derivatives that show no reactivity. [b] These molecules are not reactive at 373 K, but show reactivity at higher temperatures (473 K) with indicated rate constants between brackets.

Optical in-situ microspectroscopy: An overview of the in-situ optical microphotographs of the coffin-shaped H-ZSM-5 crystals after loading with 14 different styrene derivatives from the liquid phase is presented in Figure 2. These microphotographs were obtained at 353 K with the exception of those for **7** and **8**, which were recorded at 473 K. After reaction, the zeolite crystals exhibit colors ranging from yellow-brown through blue to pink-purple, except in the cases of **10**–**14**. Furthermore, from visual inspection of the different crystals it is evident that the coloration of the crystals is non-uniform over the crystal surface.

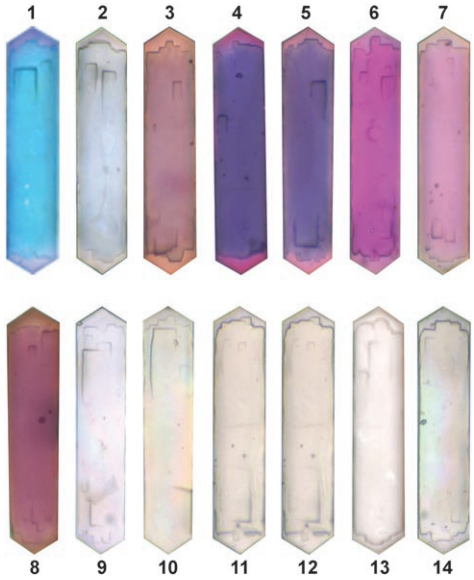

Figure 2. Optical microphotographs of the H-ZSM-5 crystals after styrene oligomerization at 353 K (**1**–**6**) and 473 K (**7**–**14**) with 14 different styrene derivatives. Snapshots were taken ≈5 min after exposure. Bold-typeface numbers correspond to the styrene compounds presented in Table 1.

The colors emerging on the crystals are indicative of the formation of different carbocation intermediates within the channel system of H-ZSM-5 materials. More specifically, as illustrated in Scheme 1, the oligomerization reaction starts

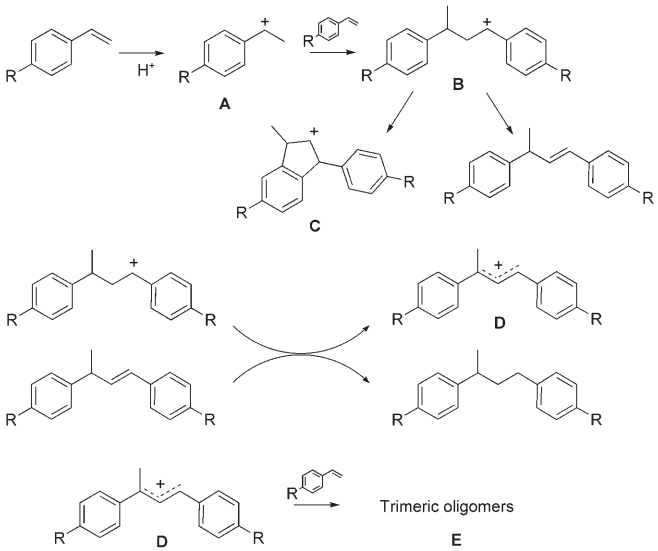

Scheme 1. Oligomerization reaction pathways of styrene derivatives on acidic zeolites. The reaction begins with protonation of styrene on the Brønsted acid sites of H-ZSM-5 (**A**). The carbocation reacts with a neutral styrene molecule, forming a secondary 1,3-bis(phenyl)-1-butylium cation (**B**), which further reacts through proton transfer and hydride shift to form the stable allylic 1,3-bis(phenyl)buten-1-ylium cation (**D**). Subsequent reactions may lead to cyclic carbocations (**C**) or higher oligomers (**E**). The absorption bands of the intermediates marked were determined for R = OCH_3: (**A**) 340, (**B**) 360, (**C**) 490 (**D**) 585 (from reference [16]) and (**E**) 620 nm (from reference [15]).

with protonation of styrene on the Brønsted acid sites of H-ZSM-5 (**A**). The carbocation reacts with a neutral styrene molecule, forming a secondary 1,3-bis(phenyl)-1-butylium cation (**B**). The latter is thermally unstable in the acidic environment of the zeolite channels, and reacts further by proton transfer and hydride shift to form the stable allylic 1,3-bis(phenyl)buten-1-ylium cation (**D**). Subsequent reactions may lead to cyclic carbocations (**C**) or higher oligomers (**E**).

Two processes can account for the difference in reactivity as revealed from the microphotographs of Figure 2. Firstly, very bulky styrene molecules, such as **10**, are not able to diffuse into the pores of the zeolite, therefore showing lack of reactivity. These observations are direct demonstrations of zeolite shape selectivity, more specifically, of reactant selectivity, as explained in classical zeolite textbooks.[17] Secondly, the stability of the initial styrene carbocation (Scheme 1) is of great importance to the catalytic activity within the pore channels, being the rate-determining step.[16] In the case of **5**, the position of the electron-withdrawing halogen atom on the aromatic ring stabilizes the carbocation by the electron density effect. In contrast, the chlorine atom, when placed at the *meta*-position, destabilizes the initial styrene carbocation, hence not showing reactivity in the case of **9**.

In line with observations reported for **1** in our recent communication,[15] close examination of all colored crystals of Figure 2 reveals that the edges and main body of these crystals exhibit different colors. These colors are associated with the presence and intensity variations of different absorption bands. This is illustrated in Figure 3, showing the UV/Vis spectra measured at the edges and main body of the crystals for the styrene derivatives that show catalytic activity. For reference purposes, Table 1 summarizes the absorption band positions determined at the edges and in the main body of the crystals for the different reactive styrene molecules.

Inspection of Table 1 and Figure 3 indicates that one absorption band dominates the edge spectra, while in the spectra from the main body of the crystals other bands at longer wavelength appear. This behavior has been previously reported for **1**,[15] for which the absorption bands were assigned to dimeric and trimeric styrene carbocations. In more detail, the band at 585 nm is due to the 1,3-bis(phenyl)buten-1-ylium cation (**D** in Scheme 1), as deduced form the comparison with the data for a nonsubstituted carbocation generated from 1,3-diphenylpropanediol upon interaction with H-ZSM-5.[16] As to the band at 630 nm, the shift to lower energies suggests an extended conjugated π system; therefore, it is reasonable to assume that the band originates from trimeric carbocations. The observation that this band arises later in time relative to that due to dimeric carbocations[15] supports this assumption. However, we could not rule out the possibility that the 635 nm band is due to a different carbocation, that is, one derived from the cyclic structure (**C** in Scheme 1), although the following discussion is in line with the original assumption. Along the same lines, we propose that for the whole series of styrene derivatives under study, higher energy absorption bands can

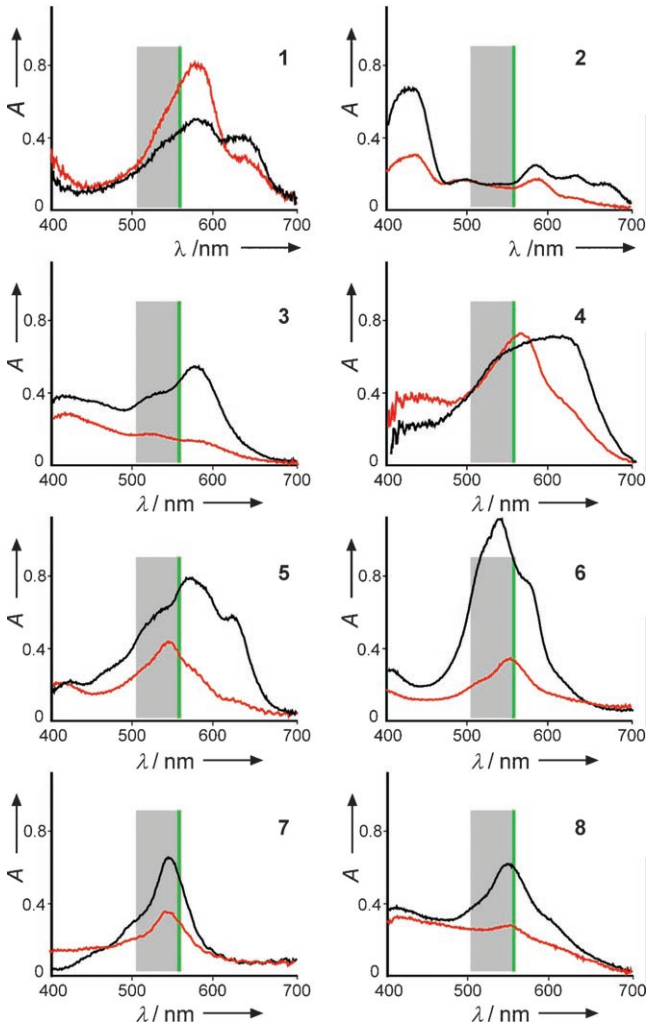

Figure 3. Optical absorption spectra of the H-ZSM-5 crystals after reaction with the catalytically active styrene derivatives at 373 K (**1**–**6**) and 473 K (**7**,**8**) at the main body (black) and edges (red) of the crystal. Bold-typeface numbers correspond to the styrene compounds presented in Table 1. The gray areas indicate the excitation wavelength range used in the fluorescence microscopy experiments (510–560 nm). The green bar indicates the laser wavelength in the confocal fluorescence measurements (561 nm).

be assigned to less-extended π systems, that is, dimeric carbocations, whereas the bands at longer wavelengths are due to the species undergoing further oligomerization, such as trimeric carbocations. This behavior may be rationalized in the frame of the recently proposed model,[15] which implies that the edge regions of the H-ZSM-5 crystals are accessible through straight pore openings, whereas in the main body of the zeolite crystal molecules can diffuse into the straight pores through openings of the sinusoidal pore system. Pore blockage at the crystal edges accounts for the preferential dimer products formation, while the more accessible amount of sinusoidal pores in the main body facilitate the formation of higher oligomers, such as trimeric products. Finally, less intense absorption bands in the optical absorption spectra of more bulky styrene compounds, for example, **2**,

are in agreement with the diffusional limitations and the less intense coloration of the zeolite material (Figure 2). Besides, the absorption spectra of **7** and **8**, which are only catalytically active at elevated temperatures (i.e. at 473 K), appear to show only one pronounced absorption band. The reason for this feature is that dimeric carbocations, formed in the straight channels of the zeolite, will become too bulky to react further and prevents the formation of higher oligomers. In other words, the absence of other higher oligomeric products observed in the spectra of **7** and **8** indicates that transition-state selectivity arguments within the zeolite-shape-selectivity concept could account for these distinct observations.

The band positions in the optical absorption spectra can be directly correlated to the different substituent groups on the aromatic ring. For example, the absorption bands for 4-methoxystyrene (**1**) are shifted by $\approx$60 nm relative to those for 4-methylstyrene (**3**). A similar trend is observed in the series 4-bromostyrene/4-chlorostyrene/4-fluorostyrene (**4**–**6**), in which substitution with more electronegative atoms leads to a stronger bathochromic shift. This finding appears to be in good agreement with effects of substitution by different groups in aromatic rings, tabulated for different compounds.[18] As a final comment on the interpretation of the absorption spectra it is important to stress that we have restricted ourselves to a brief discussion of the main trends of the UV/Vis spectra obtained, since we are fully aware that a complete and thorough assignment of the different absorption bands of the individual zeolite-stabilized styrene carbocations would require a detailed theoretical study, which is beyond the scope of the current research and will be part of a follow-up work. In other words, the given band assignments should be regarded as reasonable explanations based on the current, although limited, literature data.[16,19] However, it is comforting to notice that they are internally consistent within the set of data obtained for a large number of styrene compounds.

As the styrene oligomerization is expected to occur within the pores of the zeolite channels, one would expect that the styrene carbocation molecules, which are difficult to bend, are entrapped and aligned within the zeolite channels. Optical absorption measurements with polarized light can be used to visualize such alignment effects. When light polarization, that is, the projection of the electrical field vector, is collinear with the dipole moment vector of a photophysically active molecule, the molecule will absorb light. If the light-absorbing species are aligned on a microscopic scale, a certain range of polarization of the incident light will be absorbed. In Figure 4 in-situ microphotographs of **5** and **7** are presented, showing the dependence of the color intensity on the light polarization. One can see that when the light polarization coincides with the short crystal axis direction (θ = 90°), intense coloration is observed in the main body, while vanishing almost completely when the polarization is directed otherwise (θ = 0°). This effect is indicative of macroscopic molecule alignment within the pores of the zeolite that run along the [100] direction. In addition, Figure 4 shows the angular dependency of the absorption band intensity at the edges and main body of the crystals. The angular dependence follows the $\sin^2\theta$ law, in which θ is the angle between the long axis of the crystal and the light polarization vector. To rationalize these findings, first more insight into the microscopic structure of ZSM-5 is required, which is schematically outlined in Figure 5. H-ZSM-5 crystals possess the

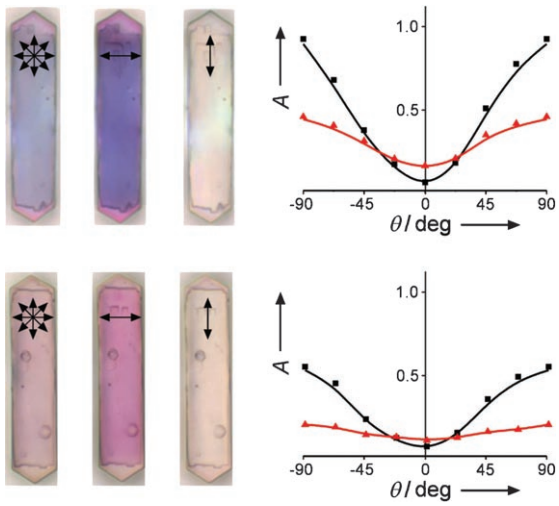

Figure 4. Left: Microphotographs of H-ZSM-5/**5** (top) and H-ZSM-5/**7** (bottom) taken with non-polarized and polarized light (light polarization is indicated by the arrows). Right: Angular dependency of the optical absorption of H-ZSM-5/**5** at 555 and 580 nm for the body (black) and edges (red) (top) and at 555 nm for the body and edges of the crystal after exposure to **7** (bottom).

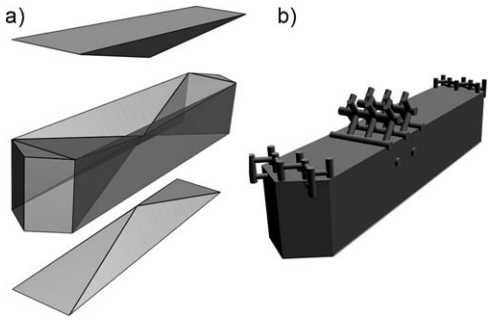

Figure 5. a) "Exploded" representation of the H-ZSM-5 crystal, showing the individual building subunits. b) Zeolite channel alignment in the different regions of the crystal. The inner zeolite framework comprised of intersecting straight and zigzag channels is accessible from the outer surface via openings of the straight pores at the edges and zigzag pores at the body of the crystal.

MFI structure with a two-dimensional pore network, made of elliptical 5.3×5.1 Å straight pores that are intersected by 5.6×5.3 Å sinusoidal or zigzag pores.[20] Furthermore, large coffin-shaped H-ZSM-5 crystals were shown to consist of three interpenetrating single crystalline subunits, of which the largest has pyramidal boundaries with the two smaller ones, which are rotated by 90° over the [001] crystallograph-

ic axis.[21–24] Using this model along with the above-mentioned angular dependence, we can infer that the light-absorbing reaction intermediates are entrapped and aligned within the straight zeolite pores. The disappearance of the optical absorption at $\theta = 0°$ implies that sinusoidal channels do not take part in accommodating the molecules, since 14 Å-long dimer molecules ought to be severely bent to fit into the 6.6 Å segments of the sinusoidal pores. Besides, upon rotation of the polarizer, the absorbance at the edges of the crystal does not change dramatically, indicating that the preferred molecule orientation is collinear with the incident light, making 90° angles with any light polarization. It is important to stress that the observed behavior upon light polarization is general for all active styrene derivatives and that polarized-light absorption unambiguously indicates that the styrene oligomerization takes place within the channels of the zeolite and not on the external surface.

Given that different parts of the crystals and therefore different pore geometries lead to distinct reaction products, which are aligned within the straight channels of the zeolite, a series of time-resolved absorption measurements would allow us to obtain more fundamental insight into the kinetics of the styrene oligomerization and thus the catalytic reactivity of each of the styrene compounds. For this purpose, time-resolved absorption spectra were first measured every second during the course of the reaction, showing the evolution of the absorption bands. This is illustrated for **5** and **7** in Figure 6. Based on the time-resolved UV/Vis spectra, rate

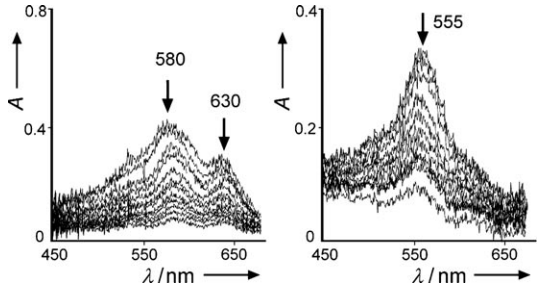

Figure 6. Time-resolved optical absorption spectra measured during the oligomerization of **5** (left) and **7** (right) at 353 and 473 K, respectively. The absorption bands are indicated by the arrows.

constants for the different reactive styrene compounds can be obtained. To do this we have taken the dimer formation kinetics as a measure of the catalytic activity. Therefore, after deconvolution of the absorption bands, the intensity of the lower wavelength band related to the dimeric styrene carbocation was plotted against time. The result of this approach is illustrated in Figure 7, as well as the time-evolution for these two styrene compounds. Fitting of the time evolution data for all reactive styrene molecules was performed using second-order kinetics; that is, styrene monomer + styrene monomer leads to a dimeric styrene carbocation. For this purpose, a second-order rate equation $d = m_0/(1+m_0kt)$ is used, in which m_0 is the initial styrene monomer concentration, d is a transient dimer concentration, and k is the kinetic rate constant for a bimolecular process.

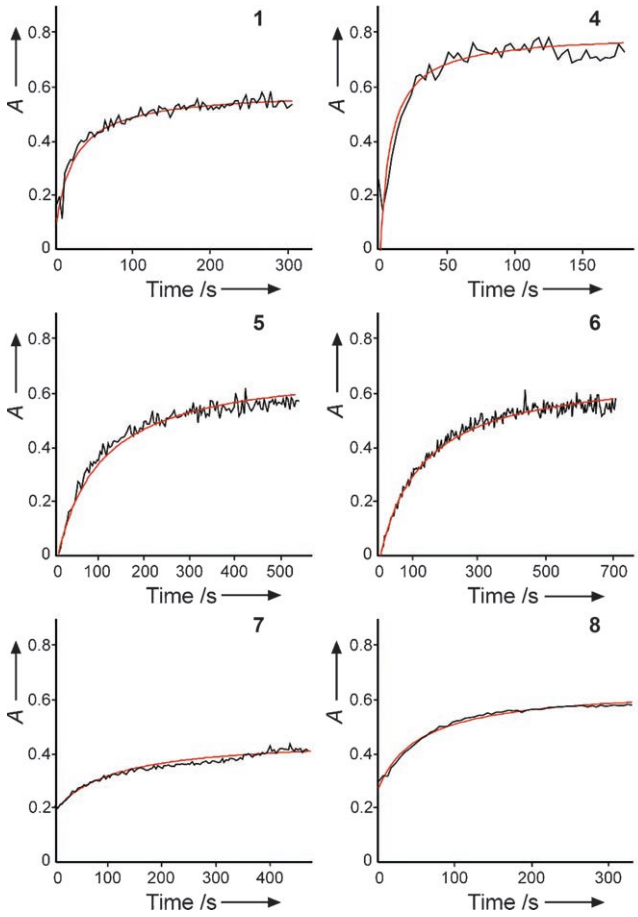

Figure 7. Time evolution of the optical absorption band assigned to the dimeric carbocation during the styrene oligomerization, taken at 373 K. The experimental profiles (black) are fitted using second-order kinetic equations (red) as described in the text. Bold-typeface numbers correspond to the styrene compounds reported in Table 1.

As evident from Figures 6 and 7, different styrene compounds not only exhibit different colors, and therefore different absorption spectra, they also show distinct reaction kinetics. These differences in dimer formation rates are summarized in Table 1, in which all 14 tested styrene compounds are listed. These reaction rate constants can be rationalized in the same manner as the microphotographs and optical absorption spectra were rationalized; that is, the stabilization of the initial styrene carbocation is the rate-determining step according to Scheme 1, and therefore donor groups substituted on the aromatic ring, for example, **1**, will contribute to a large extent to an enhanced carbocation stability. Following the same line of reasoning, strongly electron-withdrawing substituents, such as is the case for **6**, lead to a destabilization of the initial carbocation, leading to a lower reactivity. Besides, diffusion properties of the styrene molecules also influence the catalytic activity. A striking example is the comparison between **1** and **2**, which contain both electron-donating substituents. However, since the more bulky **2**

will less easily diffuse into the pores of the zeolite and suffer more steric hindrance it has a much lower reaction rate constant. Finally, as already evidenced by visual inspection of the optical microphotographs (Figure 2) very bulky compounds (e.g., **10**) will not be able to diffuse into the zeolite channels system and, as a consequence, not show any activity at all.

Fluorescence microscopy: In a parallel set of experiments, H-ZSM-5 crystals have been exposed to the styrene derivatives at elevated temperatures following the procedure identical to that described for the optical microspectroscopic studies and were consequently examined using the fluorescence microscope. From inspection of the fluorescence snapshots of the H-ZSM-5 crystals, measured inside the spectroscopic cell after the reaction with styrene, that is, after 5 min heat treatment of the styrene-loaded zeolite crystals (Figure 8), it is evident that the fluorescence intensity of the

Figure 8. Fluorescence images of the H-ZSM-5 crystals measured in the in-situ cell after styrene oligomerization taken at 373 K (**1**–**6**) and 473 K (**7**–**14**) with 14 different styrene derivatives, which are reported in Table 1. Snapshots were taken ≈5 min after the exposure.

crystals is in agreement with the strength of the coloration upon the reaction (Figure 2). Moreover, the fluorescence intensity appears to vary over the crystal surfaces, for example, in the case of **1** the edges appear to be fluorescent, whereas little light emission is observed in the main body, while the pattern for **2** reveals that the fluorescence intensity remains unchanged throughout the crystal's surface. In contrast, **3**–**8** all show little fluorescence intensity at the edges, whereas the main body of the crystals is bright. From inspection of the optical absorption spectra (Figure 3) fluorescence patterns can be straightforwardly rationalized, that is, the optical absorption in the excitation wavelength range (510–60 nm) directly corresponds to the fluorescence intensity of the crystals. For example, for **1**, the optical absorption in this excitation range is more intense at the edges, which is reflected by stronger fluorescence as compared to the main body. In the case of **2** the even fluorescence intensity over the crystal surface is in line with nearly equal (but weak) absorption in the excitation region. Finally, compounds **3**–**8** exhibit strong absorption bands in the 510–560 nm region in the main body of the crystal, which is in agreement with the distinct fluorescence pattern, featuring intense fluorescence in the main body and dark crystal edges. As the crystals were measured in the same in-situ spectroscopic cell, the fluorescence data are fully complementary with the results obtained by the optical microspectroscopic setup.

Having shown that the reaction intermediates entrapped in the zeolite channels display strong fluorescence, one can attempt to determine the three-dimensional distribution of the active species by using confocal fluorescence microscopy. Figure 9 illustrates how specific regions of the crystal

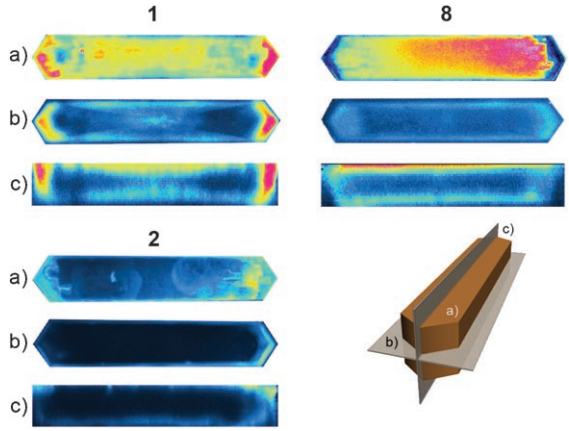

Figure 9. Confocal microscopic images of H-ZSM-5 zeolite crystals measured in the spectroscopic cell after oligomerization of **1**, **2**, and **8** at 373 K (excitation at 561 nm, detection at 580–640 nm, false color). Indices a), b), and c) correspond to the upper horizontal plane, the intermediate horizontal plane parallel to the upper plane, and the vertical intermediate plane, respectively, as shown in the model. Measurements were performed ≈5 min after the exposure.

may be selectively photoexcited, owing to the different absorption bands of the reaction intermediates being formed. To illustrate this point, confocal images for **1** and **8** are compared. One can readily see from Figure 2 that the laser excitation at 561 nm is slightly off-resonance in the case of **1**, while it matches the position of the absorption band for **8**. Differences in the optical absorption at 561 nm, as described above, accounts for the fluorescence intensity pattern, that is, brighter edges in the case of **1**, and vice versa for **8**. In view of these observations, it is important to emphasize that the confocal fluorescence images can be more accurately interpreted when optical absorption spectra are available.

Furthermore, bulkier molecules experience diffusion difficulties, as one can see from the three-dimensional volume reconstructions for **1** and **2**. In the former case the reaction

occurs in nearly the entire volume of the crystal, while in the latter only a thin near-surface layer of the catalyst is affected. Bulkier ethoxystyrene molecules, and as a consequence, dimeric carbocation of larger size lead to this effect, limiting the penetration of the reagent through the pores; this serves yet another evidence for zeolite shape selectivity. Furthermore, the internal intergrowth structure of the ZSM-5 crystals is reflected by the hourglass-shaped feature in Figure 9b for **1**, suggesting that the subunit boundaries may constitute a barrier for reactant diffusion.

Conclusions

We have demonstrated in this paper that the use of the developed in-situ optical microspectroscopic and fluorescence microscopic technique under the same reaction conditions provides very valuable insights into the catalytic processes occurring within a zeolite catalyst particle. It is shown that for the oligomerization of 14 different styrene derivatives, the reaction processes can be unambiguously rationalized. From optical microspectroscopy experiments we have shown that the distinct coloration is due to the presence of different oligomerization products in different parts of the crystal; that is, dimeric carbocations are preferentially formed at the edges, whereas higher oligomers are dominantly present in the main body of the crystal. In addition, as was shown by optical absorption measurements with polarized light, the oligomerization products appear to be aligned within the straight channels of the zeolite. Furthermore, time-resolved absorption measurements demonstrated that different substituents on the aromatic ring lead to a distinct reactivity induced by differences in carbocation stabilization and diffusion limitations. In general, more electron-donating substituents stabilize the initial carbocation and therefore show increased reactivity, whereas bulky styrene derivatives exhibit low reactivity or appear to be inactive. Fluorescence microscopy further shows that when a strong absorption band is present in the optical spectrum within the excitation range of the fluorescence microscope, strong fluorescence behavior is observed, proving the complementarity of the two in-situ microscopic techniques.

To summarize, the combined approach of in-situ optical and fluorescence microspectroscopy, which gives us the capability to study liquid-phase reactions for a broad range of reaction conditions, may become a valuable tool in catalytic studies. Furthermore, the developed microspectroscopic setup permits us to extend the scope of the method to gas-phase reactions such as the methanol-to-hydrocarbon reaction. It is expected that this tool may be applied to probe, monitor, and map structure and catalytic activity of many heterogeneous catalysts. Finally, beyond the scope of catalysis, there is a growing number of applications, such as advanced functional materials in microelectronics and optics calling for host–guest systems[25] based on single zeolite crystals.[26] For instance, sufficiently large zeolite single crystals with highly ordered structural confinement could incorporate oriented dye molecules,[27] so that the dye-loaded crystal can be used as nanoscale electronic devices, microlasers, or artificial antenna systems. Furthermore, zeolite crystals may be used to measure gas concentration, making use of anisotropic diffusion in them.[28] It is apparent that the proposed method could be applied directly to monitor various fabrication steps and operation of these devices, giving direct insight in their function.

Experimental Section

Materials and experiments: Na-ZSM-5 crystals were provided by ExxonMobil (Machelen, Belgium). A Si/Al ratio of 17 was determined with X-ray fluorescence spectroscopy. The acid form of the zeolite was obtained by triple ion exchange of Na-ZSM-5 with ammonium nitrate (10 wt%) and subsequent calcination at 723 K for 2 h. Styrene derivatives (Acros Organics and Aldrich) were used as received. The microspectroscopic analysis of the H-ZSM-5 crystals was performed in an in-situ cell (FTIR 600, Linkam Scientific Instruments) equipped with a temperature controller (Linkam TMS 93).

In-situ optical microspectroscopic setup: The setup was based on an Olympus BX41 upright research microscope with a 50×0.5 NA high-working-distance microscope objective lens. A 75 W Xenon lamp was used for illumination. The microscope was equipped with a 50/50 double viewport tube, which accommodated a CCD video camera (ColorView IIIu, Soft Imaging System GmbH) and an optical fiber mount. A 200 μm-core fiber connected the microscope to a CCD UV/Vis spectrometer (AvaSpec-2048TEC, Avantes BV). A rotatable polarizer was introduced between the objective lens and detector to separate the desirable light polarization.

In-situ confocal fluorescence microscopic setup: A Nikon Eclipse LV150 upright microscope with 50×0.55 NA dry objective lens was used for fluorescence studies. Fluorescence microphotographs were collected using 510–560 nm excitation light from the mercury source. Confocal images were acquired with a Nikon D-Eclipse C1 head connected to the laser light sources (405, 488, and 561 nm). The emission was detected with three photomultiplier tubes in the ranges 425–475, 510–550, and 575–635 nm, in order to avoid channel overlap.

Acknowledgements

We thank the Dutch National Science Foundation (NWO-CW VICI grant) and the National Research School Combination-Catalysis (NRSC-C) for financial support. Dr. Machteld Mertens (ExxonMobil, Machelen, Belgium) is acknowledged for providing the ZSM-5 crystals.

[1] A. Corma, *Chem. Rev.* **1995**, *95*, 559–614.
[2] N. Y. Chen, *Catal. Rev. Sci. Eng.* **1986**, *28*, 185–264.
[3] R. J. Quann, L. A. Green, S. A. Tabak, F. J. Krambeck, *Ind. Eng. Chem. Res.* **1988**, *27*, 565–570.
[4] S. Kotrel, J. H. Lunsford, H. Knozinger, *J. Phys. Chem. B* **2001**, *105*, 3917–3921.
[5] D. Chen, A. Gronvold, H. P. Rebo, K. Moljord, A. Holmen, *Appl. Catal. A* **1996**, *137*, L1–L8.
[6] J. C. Groen, W. Zhu, S. Brouwer, S. J. Huynink, F. Kapteijn, J. A. Moulijn, J. Perez-Ramirez, *J. Am. Chem. Soc.* **2007**, *129*, 355–360.
[7] J. A. Bergwerff, L. G. A. van de Water, T. Visser, P. de Peinder, B. R. G. Leliveld, K. P. de Jong, B. M. Weckhuysen, *Chem. Eur. J.* **2005**, *11*, 4592–4601.
[8] J. Kärger, P. Kortunov, S. Vasenkov, L. Heinke, D. B. Shah, R. A. Rakoczy, Y. Traa, J. Weitkamp, *Angew. Chem.* **2006**, *118*, 8010–8013; *Angew. Chem. Int. Ed.* **2006**, *45*, 7846–7849.

[9] P. Kortunov, C. Chmelik, J. Karger, R. A. Rakoczy, D. M. Ruthven, Y. Traa, S. Vasenkov, J. Weitkamp, *Adsorption* **2005**, *11*, 235–244.
[10] G. Müller, T. Narbeshuber, G. Mirth, J. A. Lercher, *J. Phys. Chem.* **1994**, *98*, 7436–7439.
[11] L. G. van de Water, J. A. Bergwerff, T. A. Nijhuis, K. P. de Jong, B. M. Weckhuysen, *J. Am. Chem. Soc.* **2005**, *127*, 5024–5025.
[12] M. B. J. Roeffaers, B. F. Sels, H. Uji-i, F. C. De Schryver, P. A. Jacobs, D. E. De Vos, J. Hofkens, *Nature* **2006**, *439*, 572–575.
[13] B. M. Weckhuysen, *Nature* **2006**, *439*, 548.
[14] a) M. B. J. Roeffaers, B. F. Sels, H. Uji-i, B. Blanpain, P. L'hoëst, P. A. Jacobs, F. C. De Schryver, J. Hofkens, D. E. De Vos, *Angew. Chem.* **2007**, *119*, 1736–1739; *Angew. Chem. Int. Ed.* **2007**, *46*, 1706–1709; b) M. B. J. Roeffaers, J. Hofkens, G. de Cremer, F. C. De Schryver, P. A. Jacobs, D. E. de Vos, B. F. Sels, *Catal. Today* **2007**, in press (doi:10.1016/j.cattod.2007.03.007).
[15] M. H. F. Kox, E. Stavitski, B. M. Weckhuysen, *Angew. Chem.* **2007**, *119*, 3726–3729; *Angew. Chem. Int. Ed.* **2007**, *46*, 3652–3655.
[16] F. L. Cozens, R. Bogdanova, M. Regimbald, H. Garcia, V. Marti, J. C. Scaiano, *J. Phys. Chem. B* **1997**, *101*, 6921.
[17] J. A. Martens, P. A. Jacobs, in *Introduction to Zeolite Science and Practice* (Eds.: H. van Bekkum, P. A. Jacobs, E. M. Flanigen, J. C. Jansen), Elsevier, Ansterdam, **2001**.
[18] W. Simon, T. Clerc, *Strukturaufklärung Organischer Verbindungen mit Spektroskopischen Methoden*, Akademische Verlagsgesellschaft, Frankfurt am Main, **1967**.
[19] S. S. Pollack, R. F. Sprecher, E. A. Frommell, *J. Mol. Catal.* **1991**, *66*, 195–203.
[20] G. T. Kokotailo, S. L. Lawton, D. H. Olson, W. M. Meier, *Nature* **1978**, *272*, 437–738.
[21] G. D. Price, J. J. Pluth, J. V. Smith, J. M. Bennett, R. L. Patton, *J. Am. Chem. Soc.* **1982**, *104*, 5971–5977.
[22] D. G. Hay, H. Jaeger, K. G. Wilshier, *Zeolites* **1990**, *10*, 571–576.
[23] M. Kocirik, J. Kornatowski, V. Masarik, P. Novak, A. Zikanova, J. Maixner, *Microporous Mesoporous Mater.* **1998**, *23*, 295–308.
[24] A slightly different model of large ZSM-5 crystals has been put forward based on the atomic force microscopy results (see J. R. Agger, N. Hanif, C. S. Cundy, A. P. Wade, S. Dennison, P. A. Rawlinson, M. W. Anderson, *J. Am. Chem. Soc.* **2003**, *125*, 830–839); however, this model implies the same orientation of the sinusoidal and straight channels.
[25] *Host-Guest Systems Based on Nanoporous Crystals* (Eds.: F. Laeri, F. Schüth, U. Simon, M. Wark) Wiley-VCH, Weinheim, **2003**.
[26] X. B. Yang, D. Albrecht, E. Caro, *Microporous Mesoporous Mater.* **2006**, *90*, 53–61.
[27] J. Caro, F. Marlow, M. Wubbenhorst, *Adv. Mater.* **1994**, *6*, 413–416.
[28] U. Simon, U. Flesch, W. Maunz, R. Muller, C. Plog, *Microporous Mesoporous Mater.* **1998**, *21*, 111–116.

Received: April 12, 2007
Published online: July 18, 2007

